Applied Catalysis B: Environmental 245 (2019) 20–28

Contents lists available at ScienceDirect

Applied Catalysis B: Environmental

journal homepage: www.elsevier.com/locate/apcatb

Oxygen vacancy mediated $La_{1-x}Ce_xFeO_{3-}\delta$ perovskite oxides as efficient catalysts for CWAO of acrylic acid by A-site Ce doping

Wenjing Sun[a,b], Huangzhao Wei[a], Lu yang An[c], Chengyu Jin[a,b], Huiling Wu[a,b], Zi-ang Xiong[d], Chunying Pu[e,*], Chenglin Sun[a,*]

[a] Dalian Institute of Chemical Physics, Chinese Academy of Sciences, Dalian, 116023, PR China
[b] University of Chinese Academy of Sciences, Beijing, 100049, PR China
[c] National Engineering Research Center of Coking Technology, Sinosteel Anshan Research Institute of Thermo-energy Co. Ltd., Anshan, 114044, PR China
[d] Dalian University of Technology, Dalian, 116024, PR China
[e] College of Physics and Electronic Engineering, Nanyang Normal University, Nanyang, Henan Province, 473061, PR China

ARTICLE INFO

Dedicated to the 70th anniversary of Dalian Institute of Chemical Physics, CAS.

Keywords:
Catalytic wet air oxidation
$La_{1-x}Ce_xFeO_{3-}\delta$
Synergistic mechanism
Generalized kinetic model
First-principles calculations

ABSTRACT

The influence of Ce amount on catalytic behaviour of perovskite catalysts $La_{1-x}Ce_xFeO_{3-}\delta$, prepared by coprecipitation was examined in catalytic wet air oxidation (CWAO) of high concentrated acrylic acid pollutant. The catalysts with the molar ratio of Ce/ (La + Ce) upper than 0.4 exhibit high catalytic activity, and outstanding stability. Because Ce doping into the skeleton of $LaFeO_3$ could cause the change of iron valence state as well as the change of the reactive oxygen species and oxygen vacancies of the catalyst. Three ways of O_2 involved in this reaction were considered, a synergistic mechanism of oxygen vacancies, the reversible electronic transition $Fe^{3+} \leftrightarrow Fe^{2+}$, and direct oxidization of acrylic acid. First-principles calculations revealed that the oxygen vacancy is more easily to form in the case of Ce content increasing in $La_{1-x}Ce_xFeO_{3-}\delta$, and oxygen would adsorb on oxygen vacancy to form reactive oxygen species. Consequently, the reactive oxygen species (O*) could oxidize acrylic acid. In this process, Fe ions of higher valence sate which would attack organic compounds and itself was reduced to Fe^{2+} to achieve catalytic cycles. Finally, the reaction was verified as first order, which was well explained by a proposed generalized kinetic model, in good accordance with our experimental data.

1. Introduction

Acrylic acid is an important organic synthesis raw material and synthetic resin monomer, acrylic acid and acrylic ester can be copolymerized, their polymers are used in the synthesis of resins, synthetic fibers, superabsorbent polymers, building materials, coatings and other industrial sectors. [1] Acrylic acid and its esters in the production process will produce a large amount of organic wastewater, in which chemical oxygen demand (COD) ranges from 20,000–90,000 mg L^{-1} [2]. In general, such wastewater is biodegradable and environmental hazards. The efficient removal of organic pollutants from acrylic acid industrial wastewater, therefore, has become a prime issue. So far, several treatment methods, including incineration process, wet air oxidation (WAO), biological process, supercritical water oxidation, have been developed for the removal of acrylic acid industrial wastewater. However, incineration is limited by high energy cost, air pollution and equipment corrosion [3]. The supercritical water oxidation is also high cost, and has corrosion behaviour. Biological process is not suitable for both toxic water and COD of more than 10,000 mg L^{-1}, and a large amount of activated sludge would be produced. In terms of the oxidation of various organic compounds, WAO is an effective process for removal of organic wastewater with high concentration and poor biodegradability. [4] The WAO reaction is generally carried out with or without catalyst at 120–320 °C, under pressures ranging from 0.5 to 20 MPa, [5] and has many advantages, such as the possibility of simultaneous removal of highly concentrated COD, ammonia nitrogen compounds in 2 h and production of no harmful gas and sludge. Further, the treated wastewater can be recycled. Therefore, WAO is always used to sufficiently treat various wastewaters containing complex composition, highly concentrated organics that are hard for degradation [6–8].

In the process of WAO, catalysts could mild reaction conditions, which makes WAO more economical. However, the use of homogeneous catalysts is limited by some conditions, it can only be used in acid environments, it's hard to recycle, and it would cause secondary pollution, which can be solved by using heterogeneous catalysts.

* Corresponding authors.
E-mail addresses: puchunying@126.com (C. Pu), clsun@dicp.ac.cn (C. Sun).

https://doi.org/10.1016/j.apcatb.2018.12.024
Received 3 September 2018; Received in revised form 26 November 2018; Accepted 7 December 2018
Available online 13 December 2018

Therefore, it is an urgent issue to develop a heterogeneous catalyst with high efficiency, low cost and long-term stability. [9] Among the state-of-the-art catalysts, noble metal based catalysts were generally considered to be more effective and had superior activity and satisfactory stability in the aggressive aqueous oxidative medium [10–12], but suffer from high cost (100,000–300,000 dollors m^{3-1}). To overcome this, an economic and multi-functional catalyst is needed, [13] various transition metal and rare earth metal oxides were intensively exploited as CWAO heterogeneous catalysts [14–17]. Notably, among the perovskite type catalysts, $LaMeO_3$ is the most active one. [18–21] Cu doped $LaAlO_3$ has been used as a promising catalyst in Fenton-like reactions. [22] $LaMO_3$(M═Co, Cu, Fe, Mn and Ni) is an effective catalyst for pollutant degradation. [23–26] $La_{2-x}Sr_xFeCoO_6$ exhibited thermal stability and high activity in chemical looping steam methane reforming. [27] Considering the low toxicity of Fe, $LaFeO_3$ is chosen as the substrate catalyst for CWAO. Meanwhile, cerium oxide could introduce more oxygen vacancies into the catalysts. [28] Thus this work introduce $La_{1-x}Ce_xFeO_{3-}\delta$ into CWAO process for the first time.Herein, this current work is aimed at studying the influence of Ce amount on catalyst structure and catalytic behaviour of $La_{1-x}Ce_xFeO_{3-}\delta$ CWAO process. These catalysts were prepared by the coprecipitation method. It is revealed that the optimal catalysts with the molar ratio of larger than 0.4 of Ce/(La + Ce) exhibit high catalytic activity for efficient degradation of acrylic acid by CWAO. Further, it is disclosed that, when Ce in (La + Ce) by molar ratio was upper 0.4, Ce would readily entered the skeleton of $LaFeO_3$, and thus cause efficient conversion of Fe^{2+} and Fe^{3+}, as well as the increase of reactive oxygen species and oxygen vacancies on the catalyst surface, enabling O_2 to sufficiently degrade organic pollutant. [16]

2. Experimental

2.1. Catalyst preparation

All the catalysts in this study were prepared by co precipitation method. The precipitant was 14 wt.% ammonia aqueous (100 mL), the stoichiometric $La(NO_3)_3{\cdot}6H_2O$, $Ce(NO_3)_3{\cdot}6H_2O$ and $Fe(NO_3)_3{\cdot}9H_2O$ were dissolved in 100 mL deionized water as precursors, and the total molar of La, Ce and Fe was 0.02 mol. Thereafter, the nitrate precursors (3.1 mL min^{-1}) were added into the precipitant under vigorous stirring (≈ 300 rpm). The resultant mixtures were treated at 60 °C in a water bath for 12 h. Then filtered and repeatedly washed with deionized water until the pH value of supernatant was 7. Thereafter, the powder catalyst dried at 65 °C for 24 h, and further calcined at 750 °C for 4 h.

2.2. Characterization of the catalysts

The instrument for X-ray diffraction (XRD) spectra was X'Pert PRO which is produced by PANalytical. The radiation source was Cu Kα (λ = 1.5406 Å), the current and voltage are 40 kV and 40 mA, respectively. The scan range of 2θ was 10–90°. The specific surface area of catalyst was assessed by isothermal adsorption of N_2 at 77 K, on a QUADRASORB SI instrument produced by Quantachrome Company. Fe Mössbauer spectroscopy was carried out on Topolpgic 500 A, Japan. Scanning electron microscopy (SEM) images were obtained by FE-SEM SUPRA 55 equipment by Carl Zeiss Jena. Energy dispersive X-ray spectroscopy (EDX) was carried out on an EDAX silicon-drift detector. O_2-TPD measurements were performed in a U-tube quartz micro-reactor (i.d., 4 mm). The sample weight, ranging from 0.020 to 0.025 g. Step 1, the catalyst was heated with He flow from room temperature to 800 ∘C for 77 min. Step 2, catalyst adsorbed oxygen for 60 min at 800 ∘C and then automatically cool down to room temperature in oxygen atmosphere. Step 3, repeat step 1 and 2, but in He atmosphere. And the heating rate was 10 ∘C min^{-1}. The O_2 desorption was detected by a Mass Spectrometer (Rfeiffer Vacuum, Ominstar GSD 30102) which was connected to a computer for data storage and data processing. X-ray photoelectron spectroscopy (XPS) was carried with a Thermo Scientific ESCA Lab250, Al Kα was used as the excitation source. The binding energies were corrected by C1s at 284.6 eV. H_2 temperature programmed reduction (H_2-TPR) measurements were performed in a U-tube quartz micro-reactor (i.d., 4 mm) under a 15% H_2/Ar reducing atmosphere. The sample weight, ranging from 0.020 to 0.025 g. First, the catalyst was treated with Ar flow at 300 ∘C for 60 min. Then all measurements were carried out in the range 20 ~ 900 ∘C, and the heating rate was 10 ∘C min^{-1}. The H_2 consumption was detected by a TCD detector which was connected to a computer for data storage and data processing. Transmission electron microscope (TEM) images were carried out on JEM-2100 equipment by JEOL Ltd.

2.3. Catalytic testing

Experiments were carried out in a batch reactor (TA10) of 0.5 L capacity, the reactor was equipped with a four bladed magnetically driven turbine agitators at 600 rpm. Reaction temperature remained constant during the experiments by a proportional integral differential (PID) controller. 1 mL solution was sampled from the reactor at regular intervals to analysis the substrate and total organic carbon (TOC) concentrations. In a typical run, adding 0.2 L acrylic acid solution and 1.0 g L^{-1} catalyst to the reactor, and then 3 L nitrogen was injected into the reactor to remove oxygen from the reactor. And then oxygen was charged into the reactor at the moment (time zero) of the solution was heated to the set temperature. The schematic of experimental setup is shown in Fig. **S1**. All reactions were performed under the following conditions: acrylic acid concentration = 10,000 mg L^{-1}, oxygen partial pressure = 2 MPa, reaction temperature = 240 °C, reaction time = 120 min.

2.4. Analytic methods

The concentration of acrylic acid and products were messured by high performance liquid chromatography (HPLC) produced by Dalian Elite Analytic Instruments Co., Ltd, China, equipped with an chromatographic column of Hypersil SAX (4.6 mm × 250 mm × 5 μm) and an UV detector with wavelength of 210 nm. The mobile phase was 0.01 mmol L^{-1} KH_2PO_4 and H_3PO_4 was used to adjust the pH of mobile phase to 2.5, and the flow rate was fixed at 0.8 mL min^{-1}. TOC of sample was tested by TOC Analyzer produced by TOC-V_{CPN}, Shimadzu, Japan.

The amount of Fe leaching after experiments was determined by inductively coupled plasma (ICP, PerkinElmer Optima7300DV). The pH of solution was tested by REX PHS-3C pH meter produced by Shanghai Rex Instrument Factory Co., Ltd, China, and the electrodes are calibrated before each test.

2.5. Calculation methods

$LaFeO_3$ crystalized in an orthorhombic structure at room temperature. To investigate the defect formation energies for nurtral V_O as a function of Ce atoms doping concentration, first-principles calculations are performed using the Vienna Ab initio Simulation Package with Perdew-Burke-Ernzerhof generalized gradient approximation(GGA-PBE). [29–31] A cutoff energy of 680 eV and a 2 × 2 × 2 supercell containing 160 atoms are used to optimize the structure until all residual forces remain below 0.001 eV/Å, where a Γ-centered 3 × 2 × 3 *k*-mesh is adopted for total energy calculations.

Defect formation energies are defined as the difference between the total energies of the system containing a defect and the total energy of the perfect system. To investigate defects such as vacancies or dopants that change the composition of a material, it needs to calculate the formation energy that a set of external chemical potentials of atomic species are taken into account while the atoms are removed or added the atomic system. [32] The calculated results will depend on the values of the atomic chemical potentials. For O vacancy and the Ce doping

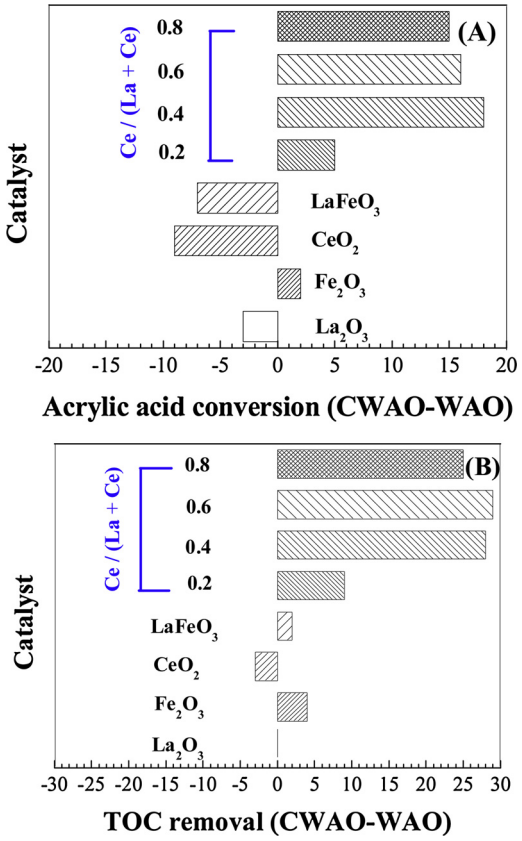

Fig. 1. WAO and CWAO of acrylic acid. (A) acrylic acid conversion; (B) TOC removal.

occupying La positions in $LaFeO_3$ crystal, defect formation energy will be evaluated as:

$$\Delta E^{f}_{Vo,\mathrm{LaCe}} = E^{tot}[La_{1-x}Ce_xFeO_3, V_O] - E^{tot}[LaFeO_3, perfect] + (1-x)\mu_{La} - x\mu_{Ce} + \frac{1}{2}\mu_{O_2}$$

Where μ_{La} and μ_{Ce} are the chemical potential of La and Ce atoms in bulk La and bulk Ce, respectively. In the present calculated work, we assume that the environment containing O_2 gas is present in all the situations. Therefore, the μ_{O_2} is the DFT total energy of the oxygen molecules.

3. Results and discussion

3.1. Catalytic activity for acrylic acid removal

Perovskite catalysts $LaFeO_3$ doped with different contents of ceria were investigated. Fig. 1 showed the acrylic acid conversion and TOC removal of different catalysts for CWAO after 120 min reaction. It can be seen that the catalysts showed greatly enhanced catalytic activity when the Ce/(La + Ce) by molar ratio were 0.4 ~ 0.8. By contrast, $LaFeO_3$, La_2O_3, CeO_2 and Fe_2O_3 showed almost no catalytic activity or a certain degree of inhibition, similar to the activity as WAO process. On the study of wet aerobic oxidation of lignin, La^{3+} and Fe^{3+} also did not present any catalytic activity. [33]

In order to understand the relationship between catalyst activity and catalyst structure and surface properties, detailed characterizations of catalysts were carried out. The results were discussed in Section 3.2 below.

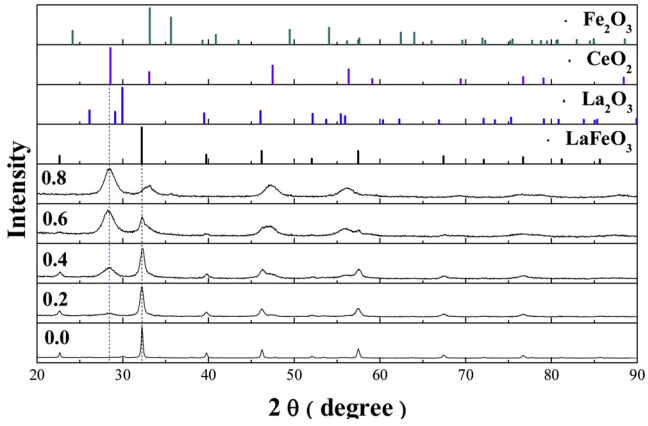

Fig. 2. XRD patterns of the catalysts with different molar ratio of Ce/ (La + Ce).

3.2. Catalyst characterization

3.2.1. XRD

The results of XRD pattern are shown in Fig. 2. According to the structural refinement, there were at most four phases among catalysts. All catalysts revealed a diffraction peak at around 32° which assigned to $LaFeO_3$ (112). Besides this, CeO_2 phase with cubic structure (reference code 01-089-8436), La_2O_3 phase with hexagonal structure (reference code 01-074-2430), and Fe_2O_3 phase with rhombohedral structure (reference code 01-087-1166) were also detected. With the increase of Ce doping content, the characteristic diffraction peaks of $LaFeO_3$ became wider and weaker gradually and shifted to large angles while the characteristic diffraction peaks of CeO_2 showed the opposite, which indicated that the content of $LaFeO_3$ decreased and crystal partical became smaller while the amount of CeO_2 increased with the increasing of Ce doping content in $LaFeO_3$ [34]. This is likely induced by the incorporation of Ce, with a smaller radius, into the skeleton of $LaFeO_3$. [35] A/B-site doping of perovskites could cause changes in physicochemical properties and catalytic activity of catalysts [36,37].

The mass fraction of each crystal phase is calculated according to adiabatic method (relative error: ± 5%). Firstly, XRD pattern of each sample was simulated by Gauss peak. Then, each crystal phase was quantitatively analyzed according to Eqs. (1)–(3), the calculation results were shown in Fig. 3(The gray line indicates that if Ce does not incorporate into the skeleton of $LaFeO_3$).When the Ce/ (La + Ce) by molar ratio was below 0.4, the content of La_2O_3 and Fe_2O_3 was lower than 5% (5% is the quantitative detection limit of XRD) and the calculated CeO_2 content was approximately the same as the theoretical amount, indicating Ce did not enter the skeleton of $LaFeO_3$. But when Ce in (La + Ce) by molar ratio was upper 0.4, the amount of CeO_2

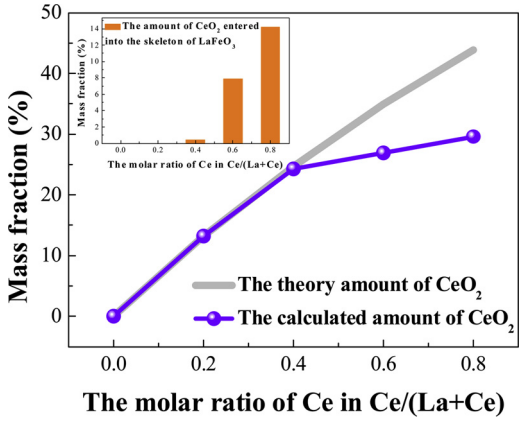

Fig. 3. XRD quantitative analysis of the catalysts.

Table 1
The specific surface area of the perovskite-like catalysts.

Ce/(La + Ce)	0	0.2	0.4	0.6	0.8
S_{BET}, $m^2 g^{-1}$	13	21	6	18	29

calculated was less than the theoretical one, suggesting Ce entered the skeleton of $LaFeO_3$. The incorporation of Ce into the framework would affect the valence state of Fe and oxygen vacancy of the catalyst, and thus affecting the catalytic activity. [38,39]

$$\sum_{i}^{n} W_i = 1 \quad (1)$$

$$I_i/I_s = K_s^i W_i/W_s \quad (2)$$

$$W_i = I_i/(K_j^i \sum_i^n (I_i/(K_j^i))) = I_i/(RIR_i \sum_i^n (I_i/RIR_i)) \quad (3)$$

(W_i: mass fraction of each crystal phase, I_i : diffraction peak intensity, *K/RIR*: ratio of intensity reference)

3.2.2. Specific surface area

The specific surface area of catalysts ranged from 6 to 29 $m^2 g^{-1}$ (Table 1). In this study, the specific surface area of catalysts prepared by coprecipitation was larger than that of perovskite catalysts prepared by Picini method (< 10 $m^2 g^{-1}$) [9,23]. Generally, specific surface area and pore structure are important parameters of solid phase catalysts. But in this work, catalytic activity has no relevance to their specific surface area.

3.2.3. Mössbauer spectra of catalyst

In order to investigate the iron oxidation state,[57] Fe Mössbauer spectroscopy was applied (**Fig. S2**), and the Mössbauer parameters were listed in **Tab. S1**. The original spectrum of catalyst can be fitted as one sextets and one paramagnetic doublet. The result suggested that there are two kinds of Fe species. The parameter of the sextets was assigned to α- Fe_2O_3 and doublet was assigned to Fe^{III} with six coordinate. [40] Another peak may contribute to $La_{0.6}Ce_{0.4}FeO_{3-}\delta$. There may have valence changes of Fe in $La_{0.6}Ce_{0.4}FeO_{3-}\delta$, which would facilitate catalytic reaction. [41] The valence state of Fe needs further analysis combined with XPS results. And the reversible electronic transition $Fe^{2+} \leftrightarrow Fe^{3+}$ could achieve catalytic cycle.

3.2.4. SEM and EDX

Morphologies and EDX analyses of perovskite-like catalysts were shown in **Fig. S3** and Table 2. The catalyst of $LaFeO_3$ (**Fig. S3-A**) showed a single morphology and it was different from that of La_2O_3, CeO_2, Fe_2O_3. When Ce/(La + Ce) by molar ratio was 0.2, it's obvious that CeO_2 was loaded on the surface of $LaFeO_3$. When the Ce /(La + Ce) by molar ratio was upper 0.4, the Fe_2O_3 appeared in the SEM diagram, as while as La_2O_3, CeO_2, and a very small amount of $LaFeO_3$. The SEM characterization verified the results of the XRD in 3.2.1 **section**.

According to the EDX results, the oxygen element content of catalyst surface was lower than the theoretical calculation, indicating that there were oxygen vacancies on the catalyst surface, that was beneficial to the catalytic reaction. [42]Because according to gas-solid L-H mechanism, oxygen would adsorb on active sites(vacant site on the catalyst) to form reactive oxygen species [43]. Finally, reactive oxygen species could oxidize organic pollutants.

3.2.5. O_2-TPD

We can infer from Fig.4 that CeO_2 and $LaFeO_3$ have almost no oxygen desorption peaks at 200–500 °C, it can be conducted that these materials have week absorption of O_2. However, as for $La_{1-x}Ce_xFeO_{3-}\delta$, it has an obvious desorption peak for oxygen at 200 ~ 500 °C, which is

Table 2
The EDX of the perovskite-like catalysts.

Ce/(La + Ce) mol/mol	Element	Found (Surface) At (%)	Calculated (Bulk) At (%)
0.0	O	42.63	60.00
	Fe	24.17	20.00
	La	32.91	20.00
	Ce	0.28	0.00
0.2	O	48.49	60.78
	Fe	26.14	19.61
	La	19.74	15.69
	Ce	5.63	3.92
0.4	O	32.61	61.54
	Fe	30.08	19.23
	La	22.39	11.54
	Ce	14.92	7.69
0.6	O	28.31	62.26
	Fe	35.17	18.87
	La	14.32	7.55
	Ce	22.20	11.32
0.8	O	47.61	62.69
	Fe	23.68	18.52
	La	6.05	3.70
	Ce	22.67	14.81

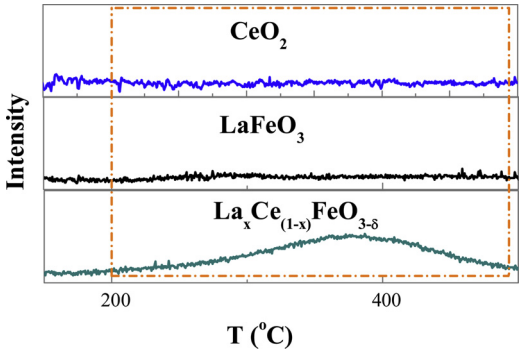

Fig. 4. O_2-TPD of catalysts.

from O_2 adsorbed on the surface oxygen vacancies, [44] that means $La_{1-x}Ce_xFeO_3$ is easier to adsorption and diffusion O_2 than CeO_2 and $LaFeO_3$. Because the reaction temperature in this work is 240 °C, so $La_{1-x}Ce_xFeO_{3-}\delta$ is easier to adsorb and activate oxygen and then effectively degradate organic matter. The result of O_2-TPD also verifies the L-H mechanism.

3.2.6. XPS

XPS analysis was carried out to study the surface chemical properties of catalysts. From Fig. 5 we can see that the peak of O1s spectra was an asymmetric peak, indicating that there are different forms of oxygen existed on the surface of catalyst. [45,46] From the peak separation results in Table 3, we can see that with the increasing of Ce doping content, the surface oxygen on the catalyst surface gradually increase, surface oxygen is often as active oxygen species [47]. So catalytic activity of $La_xCe_{1-x}FeO_{3-}\delta$ is better than that of $LaFeO_3$.

Furthermore, XPS was employed to analyzed the oxidation state of the surface Fe. The results show that there were two state of Fe on catalysts surface, that is Fe(II) and Fe(III), and Fe $2p_{3/2}$ was fitted according to literature. [48] Fig. 6 indicated that with the increasing of Ce doping content, the content of Fe(II) would increase. It was because that Ce has different valence states. Thus, Fe(II) and Fe(III) could achieve catalytic cycles.

3.2.7. TEM

It can be seen form Fig. 7 that there are many phase interface on

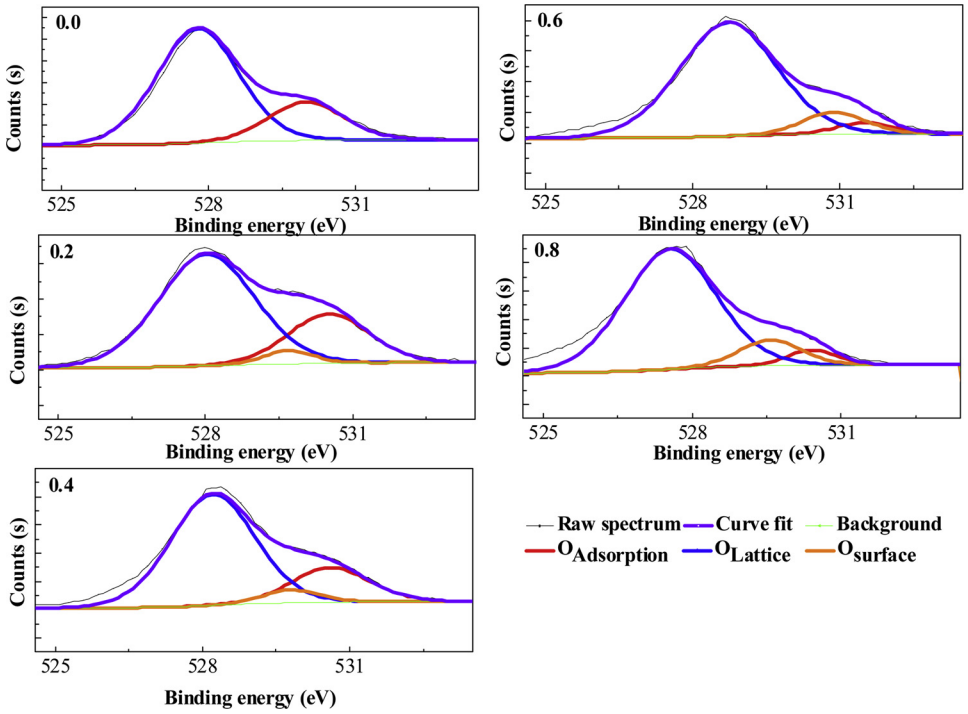

Fig. 5. The XPS O1s spectra of different catalysts.

Table 3
O XPS spectra measured for different catalysts.

Ce/(La + Ce)mol/mol	Binding energy (eV)	Assessment	Area (%)
0.0	527.78	Lattice oxygen	76.44
	——	Surface oxygen	0
	529.98	Adsorption oxygen	23.56
0.2	528.02	Lattice oxygen	69.72
	529.69	Surface oxygen	4.29
	530.51	Adsorption oxygen	25.99
0.4	528.21	Lattice oxygen	73.39
	529.79	Surface oxygen	5.64
	530.61	Adsorption oxygen	20.97
0.6	528.73	Lattice oxygen	84.56
	530.88	Surface oxygen	10.55
	531.5	Adsorption oxygen	4.89
0.8	527.56	Lattice oxygen	82.38
	529.57	Surface oxygen	12.04
	530.41	Adsorption oxygen	5.58

catalyst. And lattice defects and oxygen vacancy are easily generated at the interface. [47] In particular, it was shown that the interaction of Ce and defects could lower the activation of oxygen exchange “surface”, and thus it will enhance catalytic activity. [49] And oxygen vacancies on the catalyst surface are beneficial to the catalytic reaction, this is consistent with the above EDX results. Therefore, the incorporation of Ce into $LaFeO_3$ could improve catalytic activity.

3.3. Kinetics of acrylic acid by CWAO

Fig. **S4** showed the selective oxidation results during the reaction process and the reaction products obtained during WAO of the acrylic acid (T = 240 °C, oxygen partial pressure = 2 MPa).

Acetic acid was detected to be the only residual short-chain carboxylic acid after reaction. On the other hand, the concentration of acetic acid reached the highest after 90 min, and then gradually reduced as the reaction time extended to 120 min in this operating condition. Thus, a degradation pathway of acrylic acid is proposed as Fig.8. This is consistent with other studies, in which acetic acid is considered as a refractory product in CWAO. [50–52]

Fig. 8 shows the degradation pathway of acrylic acid. Assume that all reactions are first-order kinetics, a generalized model was proposed, [A] corresponded to the concentration of acrylic acid and [B] corresponded to the concentration of acetic acid, α was defined as the point selectivity, respectively. [53] The kinetic parameters in Eqs. (4)–(6) were obtained by a nonlinear least-squares curve fitting method using Matlab 2014®. The kinetic parameters results were listed in Table 4 **Fig. S5** exhibited the generalized model fit of the [A] and [A + B] data, the proposed kinetic model represented the experimental data well. From the dynamic point of view, the addition of catalyst greatly improved the carbon dioxide selectivity of acrylic acid, but it could not improve the degree of mineralization of acetic acid because acetic acid is hardly degraded in CWAO. When the molar ratio of Ce to (La + Ce) was 0.4, the selectivity of carbon dioxide in catalytic wet oxidation degradation of acrylic acid was the highest as well as the α value. From a kinetic point of view, the catalyst with Ce/ (La + Ce) which molar ratio equal to 0.4 was considered to be the best one.

$$ln(A/A_0) = -kt \tag{4}$$

$$k = k_1 + k_2 \tag{5}$$

$$[A + B]/[A + B]_0 = \{[k_2/(k_1 + k_2 - k_3)]exp(-k_3 t) + [(k_1 - k_3)/(k_1 + k_2 - k_3)]exp[-k_1 + k_2)t]\} \tag{6}$$

$$\alpha = k_1/k_2 \tag{7}$$

3.4. Leaching tests

To evaluate the stability of catalysts, the amount of Fe metal leached was detected. **Fig. S6** showed the results. In this study, the leaching amount of Fe was lower than 6 mg L^{-1}. The Fe leaching of catalysts in this study was much lower than that of Yang’ study (15.6 mg L^{-1}), [54] the experiment results indicated that the introduction of Ce in $LaFeO_3$ could improve the stability of perovskite-type crystal structure.

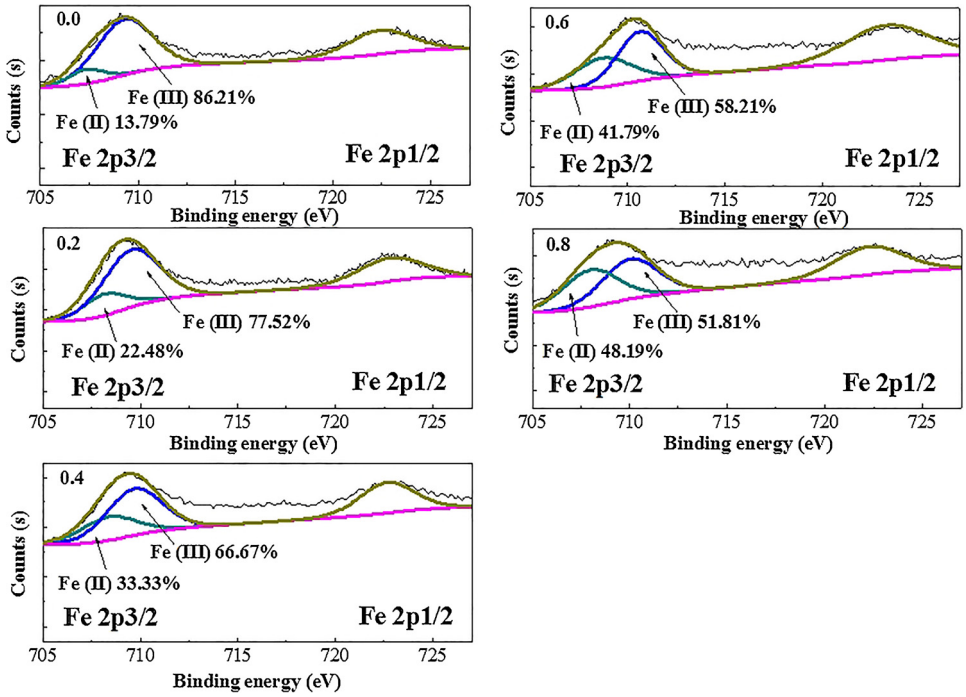

Fig. 6. The XPS Fe spectra of different catalysts.

3.5. Catalytic reaction mechanism

According to the results, a possible synergistic mechanism of CWAO for acrylic acid was proposed (Fig. 9). Oxygen vacancies and Fe^{2+}/Fe^{3+} were assumed as active sites, Fig. 9**(b)** list the oxidation valence and corresponding electron configuration of Fe metal ions in $La_{1-x}Ce_xFeO_{3-}\delta$. And these low-coordinated active atoms and adjacent oxygen ions may play the role of active sites that synergistically facilitate catalytic activity of acrylic acid oxidation. On the one hand, O_2 could be absorbed by oxygen vacancies (*) to form reactive oxygen species (O*), and reactive oxygen species (O*) would oxidize acrylic acid. On the other hand, O_2 would oxidize Fe^{2+} to Fe^{3+} under acidic conditions, and Fe^{3+} would attack organic compounds and itself was reduced to Fe^{2+} to achieve catalytic cycles. [55] At the same time, oxygen could also directly oxidize acrylic acid.

3.6. Formation energy

According to the above experimental results, the catalytic activity towards the degradation of acrylic acid in CWAO was found to strongly correlate with the lattice oxygen vacancy content. To understand the effect of Ce doping on lattice oxygen vacancy, we calculated the oxygen vacancy formation energy of $La_{1-x}Ce_xFeO_{3-}\delta$.

In Fig.10, we show the supercell structures of $LaFeO_3$ and the defect

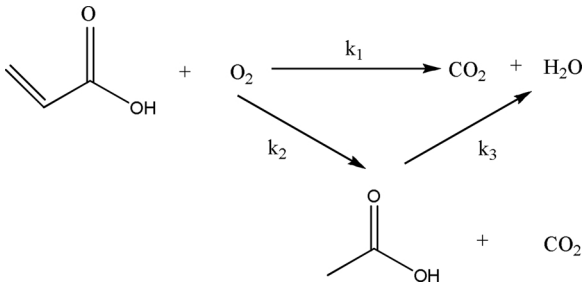

Fig. 8. The degradation pathway of acrylic acid.

Table 4
The kinetic parameters of WAO and CWAO.

Ce/(La + Ce) mol/mol	k_1 (min^{-1})	k_2(min^{-1})	k_3(min^{-1})	α
WAO	6.42E-03	3.18E-03	1.90E-03	2.02
0.0	8.51E-03	1.19E-03	0	7.17
0.2	1.15E-02	4.42E-03	0	2.61
0.4	2.05E-02	3.96E-03	0	5.17
0.6	1.79E-02	4.23E-03	0	4.23
0.8	1.69E-02	4.93E-03	0	3.42

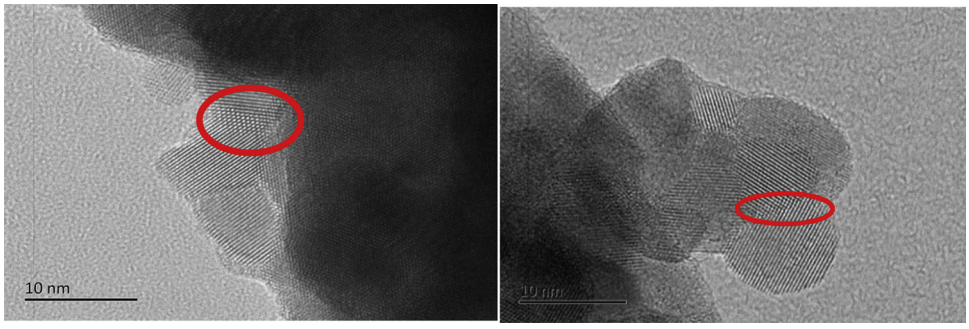

Fig. 7. TEM images of catalysts**(Ce/(La + Ce) = 0.4).**

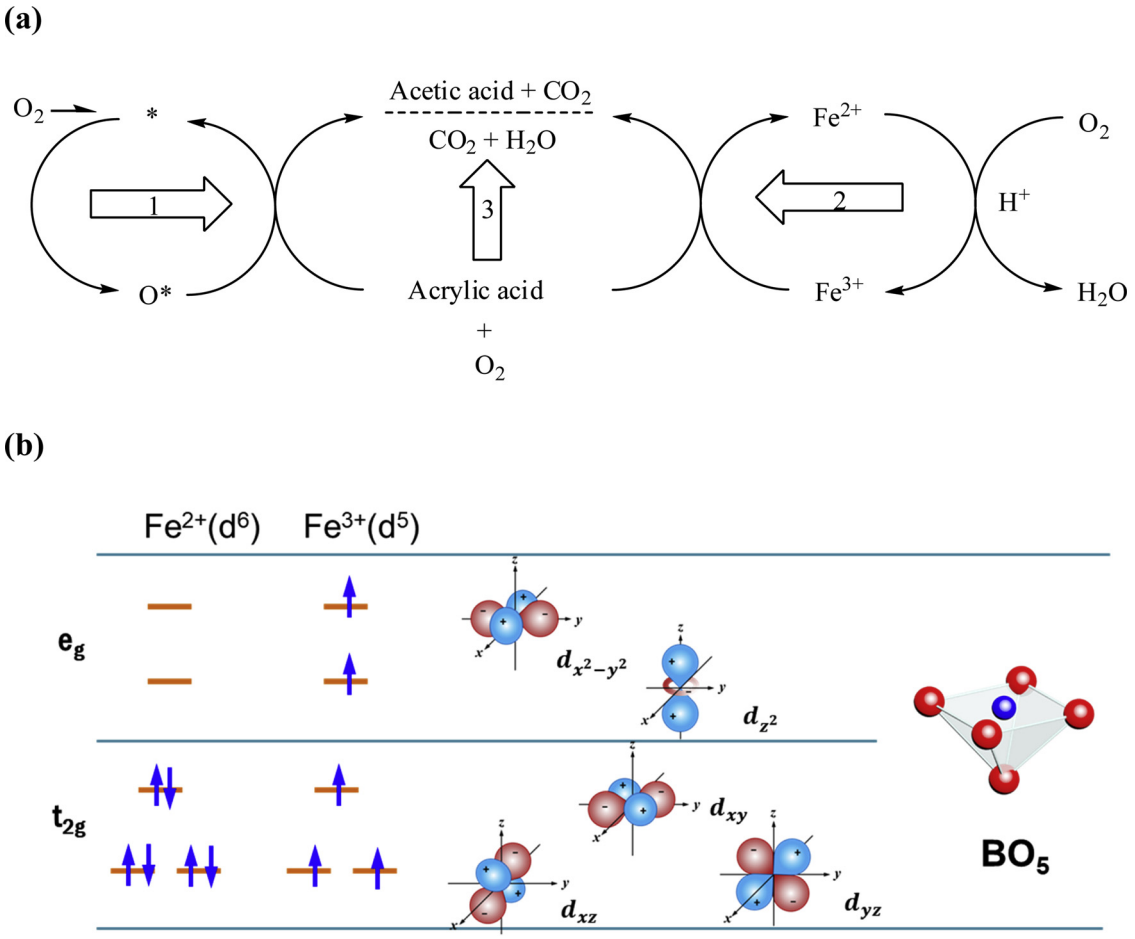

Fig. 9. (a) Scheme illustrating the possible synergistic mechanism of CWAO for acrylic acid; (b) oxidation valence and corresponding electron configuration of Fe metal ions in C_{4V} field.

formation energies for netural Vo and LaCe as a function of Ce content. It can be seen that the defect formation energy decreased linearly with the increasing of Ce doping concentration, which means that the oxygen vacancy is more easily to form in the case of Ce content increasing. By fitting to the defect formation energies using linear equation, we obtained y = -9.107x + 0.415. As we know, the low-coordinated active atoms on the surface can serve as active sites accessible to the O species. Consequently, the increase of oxygen vacancies will be beneficial for O_2 adsorption and can form reactive oxygen species (O*), these O* together with reactive oxygen species on the catalyst surface to oxidize acrylic acid. In this process, concomitantly oxidation of Fe ions to higher valence sate, which would attack organic compounds and itself was reduced to Fe^{2+} to achieve catalytic cycles.

Fig.11(a) shows the computed density of states (DOS) of the Fe d-band and its ligand O p-band, for $LaFeO_3$ and Ce-doped $LaFeO_3$, respectively. The overlap of the peaks in these two bands indicates the orbital hybridization and Fe-O binding. The strong overlap of peaks over Fermi level for the Ce-doped $LaFeO_3$ suggest more facile charge transfer process between Fe d band of B-site metal and O-2p band of the adsorbate. In addition, compared with $LaFeO_3$, Ce-doped $LaFeO_3$ oxides preserves a significant overlap of spin-down state around 0.5 eV over Fermi level, but has negligible overlap of the unoccupied spin-up states, which are anti-bonding in character, indicating the greater stability due to the Ce doping. While, highly localized electrons orbitals of La and O

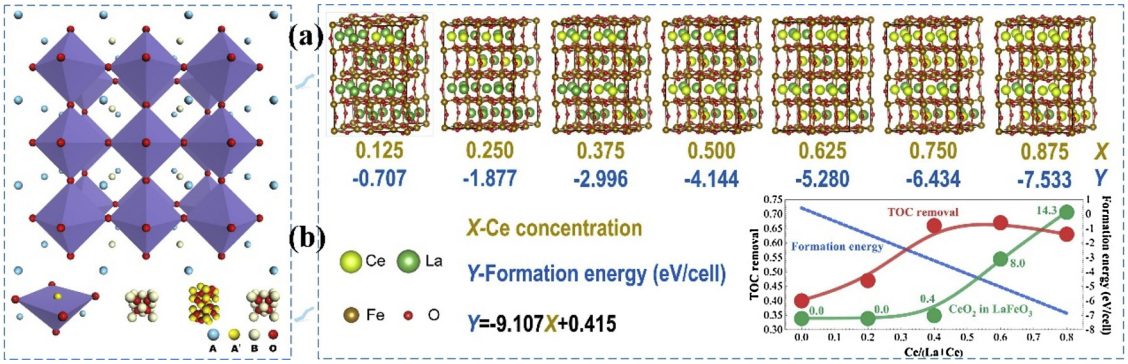

Fig. 10. (a) the 2 × 2 × 2 supercell structure of $LaFeO_3$; (b) the defect formation energy for V_O and the Ce substituted Fe sites in nutural as a function of Ce concentration.

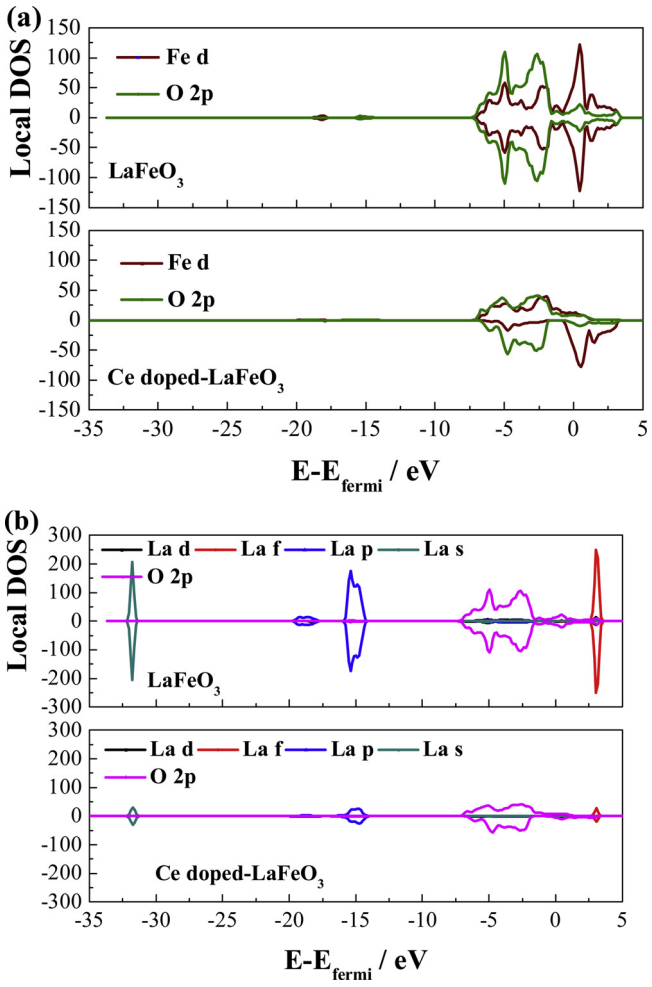

Fig. 11. (a) The density of states of d-band for the active ions Fe and the overall p-band for its ligand O, for $LaFeO_3$ and Ce-doped $LaFeO_3$, respectively; (b) The density of states of La s, p, d, f and O 2p, for $LaFeO_3$ and Ce-doped-$LaFeO_3$.

ligand, revealed stabilized framework of La in perovskite, which further explain the La^{3+} did not present any catalytic activity.

4. Conclusions

Effect of increasing Ce content on catalytic properties of perovskite catalyst $La_{1-x}Ce_xFeO_{3-}\delta$ for CWAO of acrylic acid was systematically investigated. The catalysts with the molar ratio upper than 0.4 of Ce in (La + Ce) have highly catalytic activity, stability and low cost. The catalyst with a Ce ratio of 0.4 is the most active one from a kinetic point of view. $LaFeO_3$, La_2O_3, CeO_2 and Fe_2O_3 showed the same activity as WAO and almost no catalytic activity. A synergistic mechanism of oxygen vacancies and the reversible electronic transition $Fe^{2+} \leftrightarrow Fe^{3+}$ as well as direct oxidization of acrylic acid was proposed. First-principles calculations revealed that the oxygen vacancy is more easily to form in the case of Ce content increasing in $La_{1-x}Ce_xFeO_{3-}\delta$, EDX also verified this result. Vacancy oxygen could adsorb oxygen to form reactive oxygen species according to gas-solid L-H mechanism. And XPS and H_2-TPR revealed that with the increase of Ce doping content, the content of reactive oxygen species on the catalyst surface also increases, then reactive oxygen species could oxidize organic pollutants. In addition, computed density of states (DOS) show that the catalyst could be more stable due to the Ce doping. Finally, the reaction was verified as first order, as illustrated by a generalized kinetic model, representing the experimental data well.

Conflicts of interest

There are no conflicts to declare.

Acknowledgements

This work was supported by the [DICP 1] under Grant [number DICP ZZBS201614]; [Key Programs of the Chinese Academy of Sciences 2] under Grant [number ZDRW-ZS-2016-5]; and [National Natural Science Foundation of China 3] under Grant [number 51878643].

Appendix A. Supplementary data

Supplementary material related to this article can be found, in the online version, at doi:https://doi.org/10.1016/j.apcatb.2018.12.024.

References

[1] A.M.T. Silva, R.R.N. Marques, R.M. Quinta-Ferreira, Catalysts based in cerium oxide for wet oxidation of acrylic acid in the prevention of environmental risks, Appl. Catal. B 47 (2004) 269–279.
[2] J. Wang, A. Li, T. Pan, N. Dong, Discussion on treatment processes of wastewater from acrylic acid and acrylic ester production system, China Water Wastewater 30 (2014) 68–72.
[3] H. Debellefontaine, M. Chakchouk, J.N. Foussard, D. Tissot, P. Striolo, Treatment of organic aqueous wastes: wet air oxidation and wet peroxide oxidation(R), Environ. Pollut. 92 (1996) 155–164.
[4] A.B. Ayusheev, O.P. Taran, I.A. Seryak, O.Y. Podyacheva, C. Descorme, M. Besson, L.S. Kibis, A.I. Boronin, A.I. Romanenko, Z.R. Ismagilov, V. Parmon, Ruthenium nanoparticles supported on nitrogen-doped carbon nanofibers for the catalytic wet air oxidation of phenol, Appl. Catal., B 146 (2014) 177–185.
[5] S. Yang, M. Besson, C. Descorme, Catalytic wet air oxidation of succinic acid over Ru and Pt catalysts supported on CexZr1-xO2 mixed oxides, Appl. Catal. B-Environ. 165 (2015) 1–9.
[6] S. Keav, A.E. de los Monteros, J. Barbier Jr, D. Duprez, Wet air oxidation of phenol over Pt and Ru catalysts supported on cerium-based oxides: resistance to fouling and kinetic modelling, Appl. Catal. B (2014) 402–410 150–151.
[7] C. Lousteau, H. Ayadi, C. Descorme, Aqueous phase (catalytic) wet air oxidation of ammonia: thermodynamic considerations, Appl. Catal. B 202 (2017) 12–20.
[8] I. Benhamed, L. Barthe, R. Kessas, C. Julcour, H. Delmas, Effect of transition metal impregnation on oxidative regeneration of activated carbon by catalytic wet air oxidation, Appl. Catal. B 187 (2016) 228–237.
[9] O.P. Taran, A.B. Ayusheev, O.L. Ogorodnikova, I.P. Prosvirin, L.A. Isupova, V.N. Parmon, Perovskite-like catalysts LaBO3 (B = Cu, Fe, Mn, Co, Ni) for wet peroxide oxidation of phenol, Appl. Catal. B-Environ. 180 (2016) 86–93.
[10] M. Bernardi, M. Le Du, I. Dodouche, C. Descorme, S. Deleris, E. Blanchet, M. Besson, Selective removal of the ammonium-nitrogen in ammonium acetate aqueous solutions by catalytic wet air oxidation over supported Pt catalysts, Appl. Catal., B 128 (2012) 64–71.
[11] A.C. Rabelo, A.V. Rosario, M.-L.A. Trapp, E. Rodrigues Filho, M. Forim, E.C. Pereira, Catalytic wet air oxidation of methyl Orange onto Pt and Pt-TiO2, J. Nanosci. Nanotechnol. 16 (2016) 10040–10047.
[12] S. Yang, M. Besson, C. Descorme, Catalytic wet air oxidation of succinic acid over Ru and Pt catalysts supported on CexZr1 − xO2 mixed oxides, Appl. Catal., B 165 (2015) 1–9.
[13] J. Weber, A. Thompson, J. Wilmoth, V.S. Batra, N. Janulaitis, J.R. Kastner, Effect of metal oxide redox state in red mud catalysts on ketonization of fast pyrolysis oil derived oxygenates, Appl. Catal. B 241 (2019) 430–441.
[14] Y. Zhang, Z. Zhang, Q. Yan, Q. Wang, Synthesis, characterization, and catalytic activity of alkali metal molybdate/α-MoO3 hybrids as highly efficient catalytic wet air oxidation catalysts, Appl. Catal. A 511 (2016) 47–58.
[15] S. Keav, J. Barbier, D. Duprez, Deactivation and regeneration of wet air oxidation catalysts, Catal. Sci. Technol. 1 (2011) 342.
[16] G. Ovejero, A. Rodriguez, A. Vallet, J. Garcia, Ni supported on Mg-Al oxides for continuous catalytic wet air oxidation of crystal violet, Appl. Catal. B-Environ. 125 (2012) 166–171.
[17] F. Arena, C. Italiano, A. Raneri, C. Saja, Mechanistic and kinetic insights into the wet air oxidation of phenol with oxygen (CWAO) by homogeneous and heterogeneous transition-metal catalysts, Appl. Catal. B 99 (2010) 321–328.
[18] H.B. Deng, L. Lin, Y. Sun, C.S. Pang, J.P. Zhuang, P.K. Ouyang, J.J. Li, Activity and stability of LaFeO3 catalyst in lignin catalytic wet oxidation to aromatic aldehydes, Chin. J. Catal. 29 (2008) 753–757.
[19] H.B. Deng, L. Lin, Y. Sun, C.S. Pang, J.P. Zhuang, P.K. Ouyang, Z.J. Li, S.J. Liu, Perovskite-type oxide LaMnO3: an efficient and recyclable heterogeneous catalyst for the wet aerobic oxidation of lignin to aromatic aldehydes, Catal. Lett. 126 (2008) 106–111.
[20] P. Gao, N. Li, A.Q. Wang, X.D. Wang, T. Zhang, Perovskite LaMnO3 hollow nanospheres: the synthesis and the application in catalytic wet air oxidation of phenol, Mater. Lett. 92 (2013) 173–176.
[21] K. Rusevova, R. Köferstein, M. Rosell, H.H. Richnow, F.-D. Kopinke, A. Georgi,

LaFeO3 and BiFeO3 perovskites as nanocatalysts for contaminant degradation in heterogeneous fenton-like reactions, Chem. Eng. J. 239 (2014) 322–331.
[22] H. Wang, L. Zhang, C. Hu, X. Wang, L. Lyu, G. Sheng, Enhanced degradation of organic pollutants over Cu-doped LaAlO 3 perovskite through heterogeneous Fenton-like reactions, Chem. Eng. J. 332 (2018) 572–581.
[23] K.-Y.A. Lin, Y.-C. Chen, Y.-F. Lin, LaMO3 perovskites (M = Co, Cu, Fe and Ni) as heterogeneous catalysts for activating peroxymonosulfate in water, Chem. Eng. Sci. 160 (2017) 96–105.
[24] J.-J. Li, E.-Q. Yu, S.-C. Cai, X. Chen, J. Chen, H.-P. Jia, Y.-J. Xu, Noble metal free, CeO2/LaMnO3 hybrid achieving efficient photo-thermal catalytic decomposition of volatile organic compounds under IR light, Appl. Catal. B 240 (2019) 141–152.
[25] W.Y. Hernández, D. Lopez-Gonzalez, S. Ntais, C. Zhao, A. Boréave, P. Vernoux, Silver-modified manganite and ferrite perovskites for catalyzed gasoline particulate filters, Appl. Catal. B 226 (2018) 202–212.
[26] A. Schön, J.-P. Dacquin, P. Granger, C. Dujardin, Non stoichiometric La1-yFeO3 perovskite-based catalysts as alternative to commercial three-way-catalysts? – impact of Cu and Rh doping, Appl. Catal. B 223 (2018) 167–176.
[27] K. Zhao, L. Li, A. Zheng, Z. Huang, F. He, Y. Shen, G. Wei, H. Li, Z. Zhao, Synergistic improvements in stability and performance of the double perovskite-type oxides La 2−x Sr x FeCoO 6 for chemical looping steam methane reforming, Appl. Energy 197 (2017) 393–404.
[28] X. Lin, S. Li, H. He, Z. Wu, J. Wu, L. Chen, D. Ye, M. Fu, Evolution of oxygen vacancies in MnOx-CeO2 mixed oxides for soot oxidation, Appl. Catal. B 223 (2018) 91–102.
[29] J.P. Perdew, K. Burke, M. Ernzerhof, Generalized gradient approximation made simple, Phys. Rev. Lett. 77 (1996) 3865–3868.
[30] G. Kresse, J. Furthmuller, Efficient iterative schemes for ab initio total-energy calculations using a plane-wave basis set, Phys. Rev. B 54 (1996) 11169–11186.
[31] G. Kresse, J. Furthmuller, Efficiency of ab-initio total energy calculations for metals and semiconductors using a plane-wave basis set, Comput. Mater. Sci 6 (1996) 15–50.
[32] P.G. Sundell, M.E. Bjorketun, G. Wahnstrom, Thermodynamics of doping and vacancy formation in BaZrO3 perovskite oxide from density functional calculations, Phys. Rev. B 73 (2006).
[33] J.H. Zhang, H.B. Deng, L. Lin, Wet aerobic oxidation of lignin into aromatic aldehydes catalysed by a perovskite-type oxide: LaFe(1-x)Cu(x)O(3) (x = 0, 0.1, 0.2), Molecules 14 (2009) 2747–2757.
[34] S. Yang, M. Besson, C. Descorme, Catalytic wet air oxidation of formic acid over Pt/CexZr1 − xO2 catalysts at low temperature and atmospheric pressure, Appl. Catal. B 100 (2010) 282–288.
[35] C. Ma, Y. Wen, Q. Yue, A. Li, J. Fu, N. Zhang, H. Gai, J. Zhenga, B.H. Chen, Oxygen-vacancy- promoted catalytic wet air oxidation of phenol from MnOx-CeO2, RSC Adv. 7 (2017) 27079–27088.
[36] J.A. Onrubia, B. Pereda-Ayo, U. De-La-Torre, J.R. González-Velasco, Key factors in Sr-doped LaBO3 (B = Co or Mn) perovskites for NO oxidation in efficient diesel exhaust purification, Appl. Catal. B 213 (2017) 198–210.
[37] X. Yang, Q. Gao, Z. Zhao, Y. Guo, Y. Guo, L. Wang, Y. Wang, W. Zhan, Surface tuning of noble metal doped perovskite oxide by synergistic effect of thermal treatment and acid etching: a new path to high-performance catalysts for methane combustion, Appl. Catal. B 239 (2018) 373–382.
[38] A.R. Albuquerque, A. Bruix, I.M.G. dos Santos, J.R. Sambrano, F. Illas, DFT study on Ce-doped anatase TiO2: nature of Ce3+ and Ti3+ centers triggered by oxygen vacancy formation, J. Phys. Chem. C 118 (2014) 9677–9689.
[39] N. Shehata, K. Meehan, M. Hudait, N. Jain, Control of oxygen vacancies and Ce+3 concentrations in doped ceria nanoparticles via the selection of lanthanide element, J. Nanopart. Res. 14 (2012).
[40] J. Shang, X. Guo, F. Shi, Y. Ma, F. Zhou, Y. Deng, N-substituted carbamates syntheses with alkyl carbamates as carbonyl source over Ni-promoted Fe3O4 catalyst, J. Catal. 279 (2011) 328–336.
[41] X. Li, K. Zhu, J. Pang, M. Tian, J. Liu, A.I. Rykov, M. Zheng, X. Wang, X. Zhu, Y. Huang, B. Liu, J. Wang, W. Yang, T. Zhang, Unique role of mössbauer spectroscopy in assessing structural features of heterogeneous catalysts, Appl. Catal. B 224 (2018) 518–532.
[42] H. He, X. Lin, S. Li, Z. Wu, J. Gao, J. Wu, W. Wen, D. Ye, M. Fu, The key surface species and oxygen vacancies in MnOx(0.4)-CeO2 toward repeated soot oxidation, Appl. Catal. B 223 (2018) 134–142.
[43] J.Y. Qin, K. Aika, Catalytic wet air oxidation of ammonia over alumina supported metals, Appl. Catal. B-Environ. 16 (1998) 261–268.
[44] X. Zhang, L. Liu, Z. Zhao, B. Tu, D. Ou, D. Cui, X. Wei, X. Chen, M. Cheng, Enhanced oxygen reduction activity and solid oxide fuel cell performance with a nanoparticles-loaded cathode, Nano Lett. 15 (2015) 1703–1709.
[45] S. Yang, W. Zhu, Z. Jiang, Z. Chen, J. Wang, The surface properties and the activities in catalytic wet air oxidation over CeO2-TiO2 catalysts, Appl. Surf. Sci. 252 (2006) 8499–8505.
[46] H. Chen, J. Motuzas, W. Martens, J.C. Diniz da Costa, Degradation of azo dye Orange II under dark ambient conditions by calcium strontium copper perovskite, Appl. Catal. B 221 (2018) 691–700.
[47] P. Zhang, H. Lu, Y. Zhou, L. Zhang, Z. Wu, S. Yang, H. Shi, Q. Zhu, Y. Chen, S. Dai, Mesoporous MnCeOx solid solutions for low temperature and selective oxidation of hydrocarbons, Nat. Commun. 6 (2015) 8446.
[48] C. Qi, G. Yu, J. Huang, B. Wang, Y. Wang, S. Deng, Activation of persulfate by modified drinking water treatment residuals for sulfamethoxazole degradation, Chem. Eng. J. 353 (2018) 490–498.
[49] M. Lo Faro, R.M. Reis, G.G.A. Saglietti, V.L. Oliveira, S.C. Zignani, S. Trocino, S. Maisano, E.A. Ticianelli, N. Hodnik, F. Ruiz-Zepeda, A.S. Aricò, Solid oxide fuel cells fed with dry ethanol: the effect of a perovskite protective anodic layer containing dispersed Ni-alloy @ FeOx core-shell nanoparticles, Appl. Catal. B 220 (2018) 98–110.
[50] S. Hosokawa, H. Kanai, K. Utani, Y.-i. Taniguchi, Y. Saito, S. Imamura, State of Ru on CeO2 and its catalytic activity in the wet oxidation of acetic acid, Appl. Catal. B 45 (2003) 181–187.
[51] G. Mezohegyi, B. Erjavec, R. Kaplan, A. Pintar, Removal of bisphenol A and its oxidation products from aqueous solutions by sequential catalytic wet air oxidation and biodegradation, Ind. Eng. Chem. Res. 52 (2013) 9301–9307.
[52] J. Baloyi, T. Ntho, J. Moma, A novel synthesis method of Al/Cr pillared clay and its application in the catalytic wet air oxidation of phenol, Catal. Lett. 148 (2018) 3655–3668.
[53] S.H. Lin, S.J. Ho, C.L. Wu, Kinetic and performance characteristics of wet air oxidation of high-concentration wastewater, Ind. Eng. Chem. Res. 35 (1996) 307–314.
[54] M. Yang, A. Xu, H. Du, C. Sun, C. Li, Removal of salicylic acid on perovskite-type oxide LaFeO3 catalyst in catalytic wet air oxidation process, J. Hazard. Mater. 139 (2007) 86–92.
[55] M.A.L. Rocha, G. Del Angel, G. Torres-Torres, A. Cervantes, A. Vazquez, A. Arrieta, J.N. Beltramini, Effect of the Pt oxidation state and Ce3+/Ce4+ ratio on the Pt/TiO2-CeO2 catalysts in the phenol degradation by catalytic wet air oxidation (CWAO), Catal. Today 250 (2015) 145–154.